Song et al. Nanoscale Research Letters (2015) 10:16
DOI 10.1186/s11671-014-0708-z

Nanoscale Research Letters
a SpringerOpen Journal

NANO EXPRESS Open Access

NH_3-treated WO_3 as low-cost and efficient counter electrode for dye-sensitized solar cells

Dandan Song[1], Zhao Chen[1], Peng Cui[1], Meicheng Li[1,2*], Xing Zhao[1], Yaoyao Li[1] and Lihua Chu[1]

Abstract

A novel low-cost and efficient counter electrode (CE) was obtained by treating catalytic inert tungsten trioxide (WO_3) nanomaterial in NH_3 atmosphere at elevated temperatures. The formation of tungsten oxynitride from WO_3 after NH_3 treatment, as evidenced by X-ray photoelectron spectroscopy and X-ray diffraction, increases the catalytic activity of the CE. Correspondingly, the power conversion efficiency (PCE) of the DSC is significantly increased from 0.9% for pristine WO_3 CE to 5.9% for NH_3-treated WO_3 CE. The photovoltaic performance of DSC using NH_3-treated WO_3 CE is comparable to that of DSC using standard Pt CE (with a PCE of 6.0%). In addition, it is also shown that NH_3 treatment is more efficient than H_2 or N_2 treatment in enhancing the catalytic performance of WO_3 CE. This work highlights the potential of NH_3-treated WO_3 for the application in DSCs and provides a facile method to get highly efficient and low-cost CEs from catalytic inert metal oxides.

Keywords: Tungsten trioxide (WO_3); NH_3 treatment; Counter electrode; Catalytic; Power conversion efficiency

Background

Dye-sensitized solar cells (DSCs) have attracted great attention for their low cost, simple production, and acceptable energy conversion efficiency [1,2]. It typically consists of three parts: a dye-sensitized oxide layer, electrolyte, and a counter electrode (CE). As an important component of DSCs, the CE transfers the electrons from the external circuit to the internal electrolyte and thus reduces triiodide ions to iodide ions, which realizes the continuous operation of DSCs and greatly influences the photovoltaic performance of DSCs. For achieving the high performance of DSCs, the CEs should possess high conductivity and catalytic activity [3]. High catalytic active platinized fluorine-doped tin oxide (FTO) is the most commonly used CE in DSCs. However, the high cost of scarce Pt limits the large-scale fabrication and application of DSCs, which promotes the exploration of Pt-free CEs [3-5].

Carbonaceous materials [6], conducting polymers [7], inorganic compounds (like sulfides [8], carbides [9], and nitrides [10]), and composite materials [11-13] have been reported as Pt-free materials in DSCs. The metal oxides were also studied as CEs for their facile synthesis and low cost, but the efficiencies were relatively low and not able to replace Pt [3]. These oxides may be further improved by changing their electronic structure. Hydrogen (H_2) or nitrogen (N_2) treatments have been proved to be a facile and efficient method to change the electronic structure of oxides, with which the efficiencies were improved from 0.63% to 5.43% for WO_3 by H_2 treatment and from 1.84% to 6.09% for SnO_2 by N_2 treatment [14,15]. However, the DSCs using these CEs still yield low fill factors (FF) and low efficiencies as compared to conventional Pt CEs; further improvements need to be carried out.

In this work, we demonstrated that the electronic structure of the metal oxide (WO_3) was able to be facilely changed by NH_3 treatment and its catalytic activity was also improved. The DSC using NH_3-treated WO_3 exhibits superior photovoltaic performance with a power conversion efficiency (PCE) of 5.9%, which is similar to that using standard Pt CE (6.0%) and is much higher than that using pristine WO_3 CE (0.9%). Moreover, we also demonstrated that NH_3 treatment was more efficient than H_2 or N_2 treatment in improving the performance of DSCs using WO_3-based CEs.

* Correspondence: mcli@ncepu.edu.cn
[1]State Key Laboratory of Alternate Electrical Power System with Renewable Energy Sources, School of Renewable Energy, North China Electric Power University, No. 2 Beinong Rd, Changping, Beijing 102206, China
[2]Suzhou Institute, North China Electric Power University, No. 377 Linquan Rd, Dushuhu, Suzhou 215123, China

Methods

Preparation of WO_3, NH_3-treated WO_3, and standard Pt CEs

The original WO_3 nanopowders are commercial products with a particle diameter of about 30 nm. To prepare the WO_3 slurry, 133 mg WO_3 and 20 mg ethyl cellulose are dispersed in 1 ml alpha-terpineol and then stirred for 24 h to form a fluid mixture. The yellow-green slurry was deposited on pre-cleaned FTO/glass substrates by doctor blade method to form continuous films. The films were then dried at 110°C for 30 min to remove the organic solvents and the WO_3 CEs were obtained. Atmosphere (including NH_3, H_2, and N_2)-treated WO_3 CEs were obtained by annealing the as-prepared WO_3 CEs in different atmospheres at 480°C for 2 h. Standard Pt CE was also fabricated by sputtering thermodecomposition of H_2PtCl_6 on pre-cleaned FTO/glass at 450°C for 20 min.

Fabrication of DSCs

TiO_2 films were prepared by doctor blading of TiO_2 nanoparticle (P25) slurry on FTO/glass substrates. All of the TiO_2 films were post-treated with $TiCl_4$. After calcination, the TiO_2 films were immersed in a 0.3 mmol/l ethanol solution of N719 dye for 24 h. The DSCs were fabricated by assembling dye-sensitized TiO_2 photoanodes with as-fabricated CEs using 30-μm-thick Surlyn (DuPont, Wilmington, DE, USA). I^-/I_3^- electrolyte with acetonitrile as the solvent was used. The active area of solar cells was about 4 mm × 4 mm. Symmetric cells for electrochemical measurements were fabricated by assembling two identical CEs together using 30-μm-thick Surlyn.

Characterization methods

The structure and morphology properties of the samples were measured by X-ray diffraction (XRD; XRD-6000, Shimadzu Corp., Kyoto, Japan) and scanning electron microscopy (SEM; S-4800, Ltd., Tokyo, Japan). The element distribution was tested by X-ray photoelectron spectroscopy (XPS) and electron diffraction spectroscopy (EDS). The photovoltaic performance of DSCs was characterized using a source meter (2400, Keithley Instruments, Inc., Beijing, China) under AM 1.5G irradiation (100 mW/cm^2) generated by a solar simulator (XES-301S + EL-100, San-ei Electric Co., Ltd., Osaka, Japan). Electrochemical impedance spectroscopy (EIS) was carried out using the electrochemical workstation (CHI660D), performed on symmetric cells.

Results and discussion

Figure 1 shows the XRD patterns of the pristine WO_3 and NH_3-treated WO_3 products. The most intensive diffraction peaks of the pristine WO_3 match well with the typical monoclinic WO_3 (JCPDS no. 431035). However, after NH_3 treatment, the locations of the intensive diffraction peaks are totally changed, which match well with the tungsten oxynitride (WO*x*N*y*, JCPDS no. 251254). Correspondingly, the color of WO_3 is also changed from yellow to black after NH_3 treatment (insets of Figure 1).

However, as cubic tungsten nitride (WN, JCPDS no. 751012) and WO*x*N*y* (JCPDS No. 251254) have almost identical lattice structures and hence diffraction peaks in the XRD pattern, it is difficult to distinguish them only with XRD results [16-18]. Hence, the surface chemical

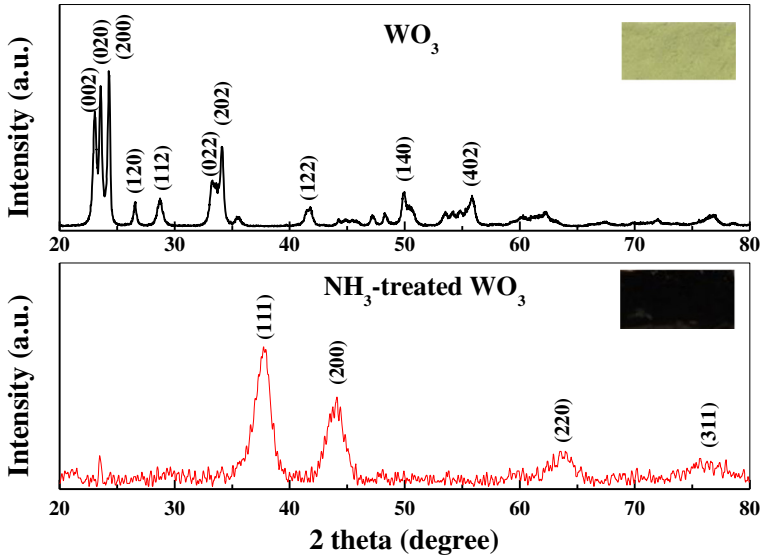

Figure 1 XRD curves of pristine WO_3 and NH_3-treated WO_3 samples. The insets show the digital pictures of WO_3 and NH_3-treated WO_3 powders.

element composition was studied by XPS. Figure 2a shows the N 1 s XPS spectra of WO_3 and NH_3-treated WO_3 samples. In the condition of WO_3, the low-intensity and relatively broad peak at 400.2 eV can be ascribed to the γ-N state caused by chemisorbed nitrogen molecules on the WO_3 surface [19]. In the condition of NH_3-treated WO_3, the high-intensity peak at 396.9 eV can be observed, which corresponds to the β-N state and is essentially the atomic N [18,19], demonstrating that nitrogen has been successfully incorporated into the WO_3.

The W 4f XPS spectra of WO_3 and NH_3-treated WO_3 samples are shown in Figure 2b. The peaks at 35.77 eV (W $4f_{7/2}$) and 37.97 eV (W $4f_{5/2}$) from WO_3 can be ascribed to the binding energy of high oxidation state of W. In comparison, one additional peak at 33.32 eV ($W4f_{7/2}$), which is associated with lower oxidation states of W, can be observed from the NH_3-treated WO_3 sample, indicating the formation of W-N bonds in NH_3-treated WO_3 as might

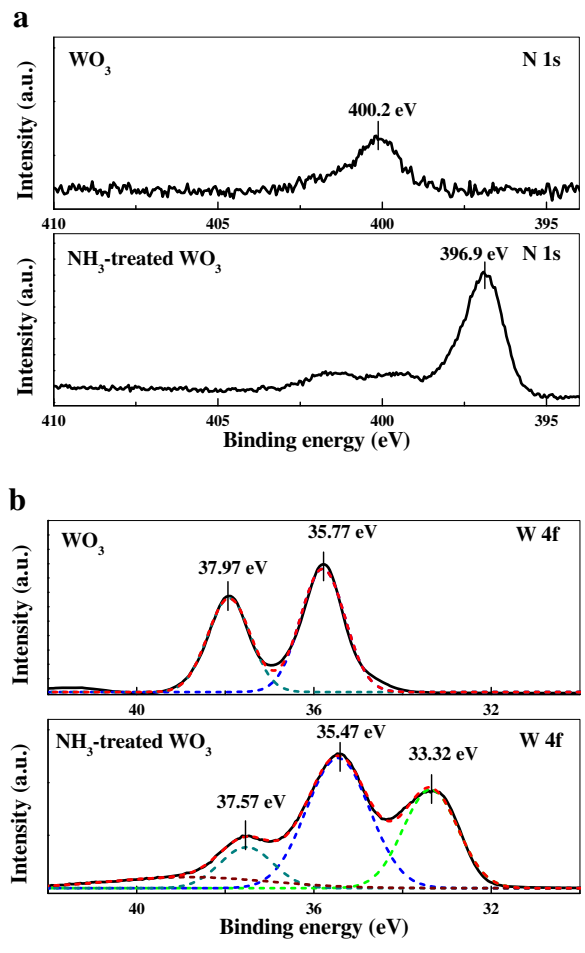

Figure 2 N 1 s (a) and W 4f (b) XPS spectra of WO_3 and NH_3-treated WO_3 samples. The solid lines represent the measured data, and the dashed lines represent the Gaussian fitted curves.

be expected in tungsten oxynitrides [18]. In addition, the peaks located at 35.37 and 37.47 eV from NH_3-treated WO_3 are lower compared with those from the pristine WO_3 (35.77 and 37.97 eV), which probably result from the existence of less electronegative atoms into the oxide lattice considering the fact that N has smaller electronegativity (3.04) than O (3.44). From the above results, it can be concluded that WO*x*N*y*, other than tungsten nitrides, were formed, as in good accordance with the previous XRD analysis.

The morphology of the two different WO_3 CEs was also characterized by SEM. Figure 3a,b presents the top-view SEM images of WO_3 and NH_3-treated WO_3 CE, respectively. It is clear that these two CEs are both porous which is useful for the diffusion of iodide/triiodide redox couples in the films. The EDS patterns shown in Figure 3c,d from these two CEs are quite different. No signal of N can be observed in WO_3 CE (Figure 3c), while the signal of N is obvious in NH_3-treated WO_3 (Figure 3d). In addition, the atomic ratio of O to W is decreased from 3.19 to 1.05 by NH_3 treatment, suggesting that the oxygen sites are partially substituted by nitrogen atoms in reductive NH_3 atmosphere.

To study the kinetics of the catalytic property of the CEs, EIS was carried out on symmetric cells fabricated with two identical CEs. Nyquist plots from WO_3, NH_3-treated WO_3, and standard Pt CEs are shown in Figure 4, and the equivalent circuit of the symmetric cells is shown in the inset of Figure 4. The high-frequency intercept at the real axis (Z') represents the series resistance (R_S). Two arcs can be seen in the Nyquist plots, which correspond to the charge transfer resistance (R_{CT}) and the capacitance (CPE) at electrolyte/electrode interface (the left arc in the high-frequency region) and the Nernst diffusion impedance (Z_N) of redox sites in the electrolyte (the right arc in the low-frequency region), respectively [3,10,12]. The simulated R_{CT} of the NH_3-treated WO_3 CEs is 9.2 Ω, similar to that of the Pt electrode (9.3 Ω). In regard to the pristine WO_3 CE, the electrocatalytic activity is lower according to its large R_{CT} (>100 Ω). The simulated Z_N of Pt CE is 4.7 Ω, while those of WO_3 CE and NH_3-treated WO_3 CE are higher probably due to combination of the Nernst diffusion impedance and the porous diffusion impedance in the porous WO_3-based CEs. Nevertheless, the similar R_{CT} value of NH_3-treated WO_3 and standard Pt CE highlights the superior electrocatalytic activity of NH_3-treated WO_3 CE for the reduction of triiodide ions, which provides a crucial precondition for replacing the Pt CE with the NH_3-treated WO_3 CE in DSCs.

Figure 5 presents the photocurrent density-voltage (*J-V*) curves of the DSCs using WO_3, NH_3-treated WO_3, and standard Pt CEs. The detailed photovoltaic parameters from the *J-V* curves are summarized in Table 1. The DSC

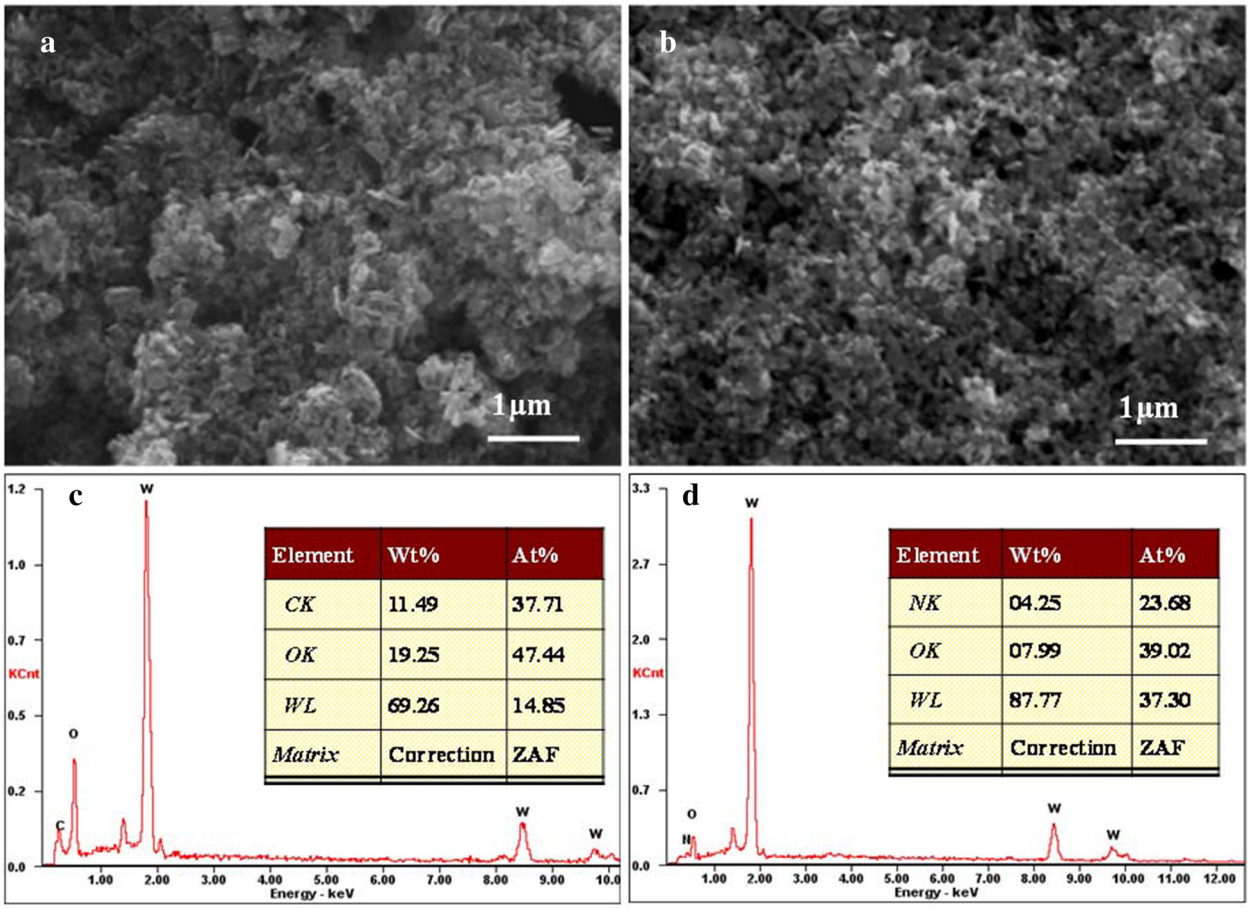

Figure 3 SEM images (a, b) and EDS spectra (c, d) of WO_3 CE and NH_3-treated WO_3 CE. Insets in **(c)** and **(d)** are the corresponding detailed elemental distribution.

with WO_3 CE has a poor photovoltaic performance with a low FF of 17.6% and a low short-circuit current density (J_{sc}) of 12.8 mA/cm^2. With NH_3 treatment, the related DSC shows an improved photovoltaic performance with a FF of 62.0% and a J_{sc} of 14.0 mA/cm^2. Therefore, the PCE of DSC using NH_3-treated WO_3 CE (5.9%) is much higher than that of DSC using pristine WO_3 CE (0.9%). In comparison, the DSC with standard Pt CE has also been characterized and shows a similar PCE (6.0%) to that with NH_3-treated WO_3 CE, demonstrating the potential of NH_3-treated WO_3 CEs used as Pt substituents.

It is worth noting that the FF and PCE obtained from DSC using the NH_3-treated WO_3 CE are also relatively higher in comparison with those from DSC using tungsten nitrides [10]. In addition, the obtained FF and PCE from DSC using NH_3-treated WO_3 CE are also higher than those from DSC using H_2- or N_2-treated WO_3 CE. The N_2- and H_2-treated WO_3 were also fabricated under the same conditions with NH_3-treated WO_3 and used as CEs for DSCs. As shown in Figure 6, the DSC using N_2-treated WO_3 CE yields a lower FF of 45.6% and a PCE of 3.9%. The DSC using H_2-treated WO_3 CE shows a FF of 50.4% which is similar to previous report [14] and a PCE of 4.5%. The DSC using NH_3-treated WO_3 CE exhibits the best performance with the highest FF and PCE, demonstrating the great advantage of NH_3 treatment for preparing highly efficient and low-cost CEs.

The excellent performance of NH_3-treated WO_3 CE can be ascribed to the change of electronic structure from tungsten oxide to tungsten oxynitride by NH_3 treatment. NH_3-treated WO_3 CE possesses similar W-N bonds to tungsten nitride which is a catalytic active site for the reduction of triiodide [10,20]; hence, it is also able to provide Pt-like electrocatalytic properties. Meanwhile, as the reduction ability of NH_3 also provides a reduction atmosphere for WO_3, which will create oxygen vacancies as similar to the case of H_2 treatment [14], the catalytic activity can also be improved in the presence of oxygen vacancies. Therefore, NH_3-treated WO_3 CE exhibits the best performance among the WO_3 CEs treated in different atmospheres.

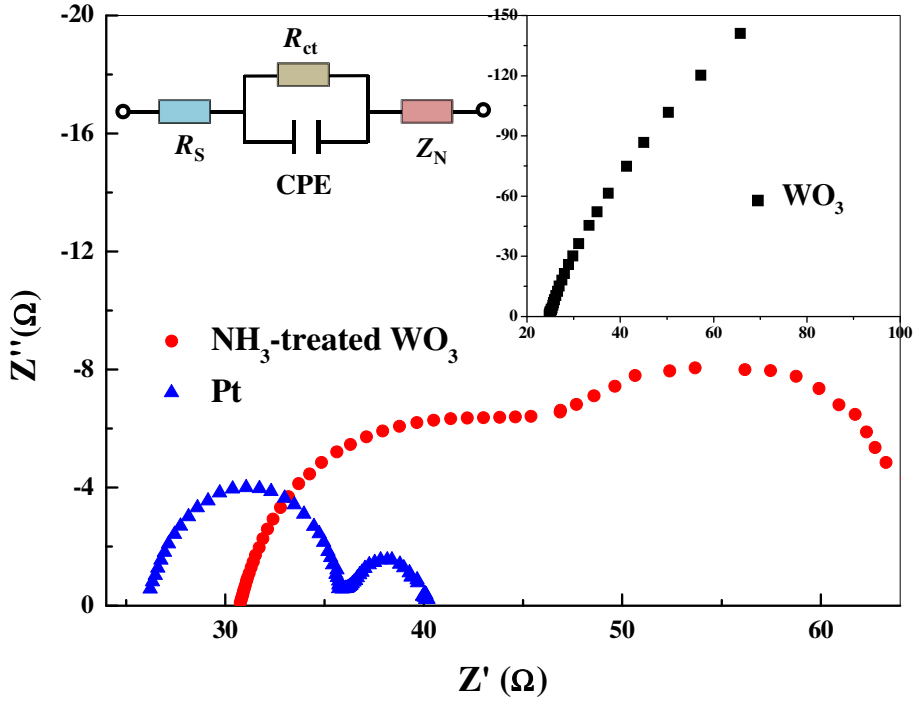

Figure 4 Nyquist plots from symmetric cells with different counter electrodes. The inset shows the equivalent circuit of the symmetric cells.

Moreover, NH_3 treatment may also vary the energy level of WO_3 by introducing oxygen vacancies. As the conduction band level of WO_3 (approximately 0.7 V versus normal hydrogen electrode (NHE)) is larger than the potential of I^-/I_3^- (approximately 0.3 V versus NHE), the overpotential for triiodide reduction in WO_3 CE will be inevitable, leading to a low V_{OC} in DSCs using WO_3 CE (as shown in Figure 5). However, the V_{OC} values of DSCs using Pt CE and NH_3-treated WO_3 CE are nearly identical, which indicates that the overpotential for triiodide reduction in NH_3-treated WO_3 CE is negligible and the Fermi level of WO_3 is varied by NH_3 treatment. It is proposed that hydrogen incorporation in WO_3 favors the occupation of gap states near the Fermi level and the maintenance of a high work function, which facilitate the charge transport and enhance charge extraction in organic solar cells [21]. NH_3 treatment may also play a similar role in affecting the electronic structure of WO_3 and can be explored as a hole-extracting layer for organic solar cells.

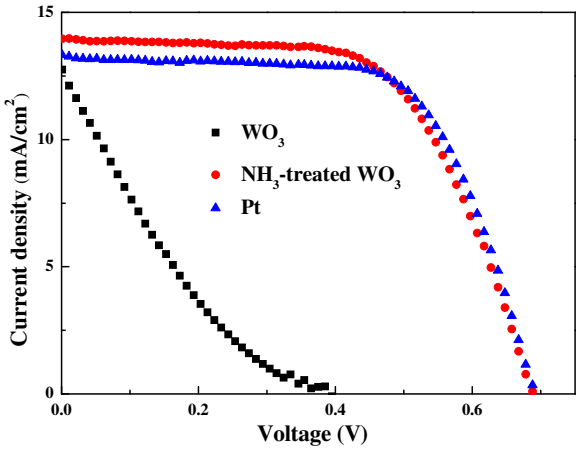

Figure 5 Photocurrent density-voltage curves of DSCs using WO_3, NH_3-treated WO_3, and standard Pt CEs under 100 mW/cm² irradiation.

Conclusions

In conclusion, it is demonstrated that NH_3 treatment can significantly improve the catalytic performance of WO_3 in the use of CE material for DSCs. By annealing commercial WO_3 in a NH_3 atmosphere, the oxygen atoms in WO_3 can be partially substituted by nitrogen to form

Table 1 Photovoltaic parameters of DSCs using WO_3, NH_3-treated WO_3, and standard Pt CE

CEs	J_{sc} (mA/cm²)	V_{oc} (V)	FF (%)	PCE (%)
WO3	12.8	0.40	17.6	0.9
NH3-treated WO3	14.0	0.68	62.0	5.9
Pt	13.3	0.69	65.4	6.0

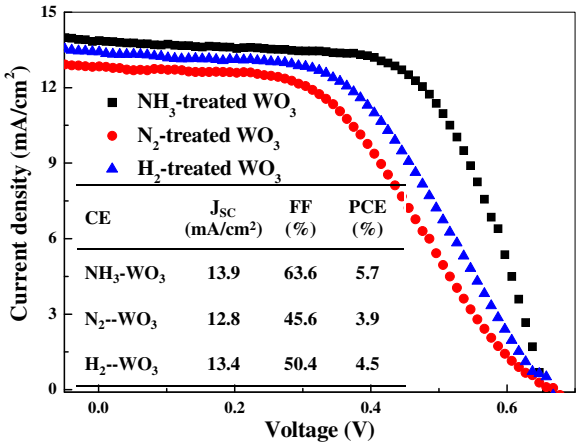

Figure 6 Photocurrent density-voltage curves of DSCs using WO_3 CEs treated under different atmospheres under 100 mW/cm^2 irradiation.

tungsten oxynitrides, which obviously enhance the catalytic activity of the CEs. Correspondingly, the DSC using NH_3-treated WO_3 CE exhibits excellent performance, which is comparable to the DSC using standard Pt CE. The findings in this work also provide new insights into the exploration of low-cost and highly efficient CE materials with metal oxynitrides for DSCs.

Competing interests
The authors declare that they have no competing interests.

Authors' contributions
DS conceived the research idea, participated in the experimental process, and drafted the manuscript. ZC did most of the experiments and participated in drafting the manuscript. PC did part of the experiments. ML supervised the design and realization of the study. XZ, YL, and LC took part in the discussion of the research. All authors read and approved the final manuscript.

Acknowledgements
This work was supported partially by the National Natural Science Foundation of China (Grant nos. 51372082, 51172069, 50972032, 61204064, 51202067, and 91333122), Ph.D. Programs Foundation of Ministry of Education of China (Grant nos. 20110036110006, 20120036120006, and 20130036110012), Science and Technology Program Foundation of Suzhou City (SYG201215), and the Fundamental Research Funds for the Central Universities.

Received: 6 October 2014 Accepted: 23 December 2014
Published online: 28 January 2015

References
1. O'Regan B, Gratzel M. A low-cost, high-efficiency solar cell based on dye-sensitized colloidal TiO_2 films. Nature. 1991;353:737–40.
2. Hagfeldt A, Boschloo G, Sun L, Kloo L, Pettersson H. Dye-sensitized solar cells. Chem Rev. 2010;110:6595–663.
3. Wu M, Lin X, Wang Y, Wang L, Guo W, Qi D, et al. Economical Pt-free catalysts for counter electrodes of dye-sensitized solar cells. J Am Chem Soc. 2012;134:3419–28.
4. Hou Y, Wang D, Yang XH, Fang WQ, Zhang B, Wang HF, et al. Rational screening low-cost counter electrodes for dye-sensitized solar cells. Nat Commun. 2013;4:1583.
5. Ahmad S, Guillen E, Kavan L, Grätzel M, Nazeeruddin MK. Metal free sensitizer and catalyst for dye sensitized solar cells. Energ Environ Sci. 2013;6:3439–66.
6. Cha SI, Koo BK, Seo SH, Lee DY. Pt-free transparent counter electrodes for dye-sensitized solar cells prepared from carbon nanotube micro-balls. J Mater Chem. 2010;20:659–62.
7. Zhao X, Li M, Song D, Cui P, Zhang Z, Zhao Y, et al. A novel hierarchical Pt- and FTO-free counter electrode for dye-sensitized solar cell. Nanoscale Res Lett. 2014;9:202.
8. Xin X, He M, Han W, Jung J, Lin Z. Low-cost copper zinc tin sulfide counter electrodes for high-efficiency dye-sensitized solar cells. Angew Chem Int Ed. 2011;50:11739–42.
9. Wu M, Mu L, Wang Y, Lin Y, Guo H, Ma T. One-step synthesis of nano-scaled tungsten oxides and carbides for dye-sensitized solar cells as counter electrode catalysts. J Mater Chem A. 2013;1:7519.
10. Li GR, Song J, Pan GL, Gao XP. Highly Pt-like electrocatalytic activity of transition metal nitrides for dye-sensitized solar cells. Energy Environ Sci. 2011;4:1680.
11. Song D, Li M, Jiang Y, Chen Z, Bai F, Li Y, et al. Facile fabrication of MoS_2/PEDOT–PSS composites as low-cost and efficient counter electrodes for dye-sensitized solar cells. J Photochem Photobio A Chem. 2014;279:47–51.
12. Song D, Li M, Li Y, Zhao X, Jiang B, Jiang Y. Highly transparent and efficient counter electrode using SiO_2/PEDOT–PSS composite for bifacial dye-sensitized solar cells. ACS Appl Mater Interfaces. 2014;6:7126–32.
13. Song D, Li M, Wang T, Fu P, Li Y, Jiang B, et al. Dye-sensitized solar cells using nanomaterial/PEDOT–PSS composite counter electrodes: effect of the electronic and structural properties of nanomaterials. J Photochem Photobio A Chem. 2014;293:26–31.
14. Cheng L, Hou Y, Zhang B, Yang S, Guo JW, Wu L, et al. Hydrogen-treated commercial WO_3 as an efficient electrocatalyst for triiodide reduction in dye-sensitized solar cells. Chem Commun. 2013;49:5945.
15. Wu M, Lin X, Guo W, Wang Y, Chu L, Ma T, et al. Great improvement of catalytic activity of oxide counter electrodes fabricated in N_2 atmosphere for dye-sensitized solar cells. Chem Commun. 2013;49:1058.
16. Xu F, Fahmi A, Zhao Y, Xia Y, Zhu Y. Patterned growth of tungsten oxynitride nanorods from Au-coated W foil. Nanoscale. 2012;4:7031–7.
17. Cho DH, Chang TS, Shin CH. Variations in the surface structure and composition of tungsten oxynitride catalyst caused by exposure to air. Catalysis Lett. 2000;67:163–9.
18. Zhao YM, Hu WB, Xia YD, Smith EF, Zhu YQ, Dunnillc CW, et al. Preparation and characterization of tungsten oxynitride nanowires. J Mater Chem. 2007;17:4436–40.
19. Saha NC, Tompkins HG. Titanium nitride oxidation chemistry: an X-ray photoelectron spectroscopy study. J Appl Phys. 1992;72:3072.
20. Wu M, Zhang Q, Xiao J, Ma C, Lin X, Miao C, et al. Two flexible counter electrodes based on molybdenum and tungsten nitrides for dye-sensitized solar cells. J Mater Chem. 2011;21:10761–6.
21. Vasilopoulou M, Soultati A, Georgiadou DG, Stergiopoulos T, Palilis LC, Kennou S, et al. Hydrogenated under-stoichiometric tungsten oxide anode interlayers for efficient and stable organic photovoltaics. J Mater Chem A. 2014;2:1738–49.